Journal of Power Sources 196 (2011) 371–378

Contents lists available at ScienceDirect

Journal of Power Sources

journal homepage: www.elsevier.com/locate/jpowsour

Influence of polystyrene/phenyl substituents in precursors on microstructures of Si–O–C composite anodes for lithium-ion batteries

Hiroshi Fukui [a], Hisashi Ohsuka [a], Takakazu Hino [a], Kiyoshi Kanamura [b,*]

[a] Dow Corning Toray Company, Ltd., Chigusa-Kaigan, Ichihara 299-0108, Japan
[b] Department of Applied Chemistry, Tokyo Metropolitan University, Minami-Osawa, Hachioji, Tokyo 192-0397, Japan

ARTICLE INFO

Article history:
Received 14 May 2010
Received in revised form 21 June 2010
Accepted 21 June 2010
Available online 30 June 2010

Keywords:
Silicon oxycarbide
Polysilane
Micropore
Rechargeable lithium battery
Composite anode material

ABSTRACT

Pyrolysis of methylphenyl-substituted branched polysilane–polystyrene polymer blends led to the formation of silicon oxycarbide (Si–O–C) glasses with microstructures similar to those found in hard carbon. Electrochemical measurements showed that the Si–O–C composite materials had lithium storage capacities of more than 500 mA h g^{-1}, with a short but characteristic pseudo-voltage plateau at ca. 0.1 V upon delithiation. This voltage plateau indicates the existence of micropores where less-ionic lithium species can be formed, as seen in the case of hard carbon. The micropores were minor electrochemically active sites but led to an increase in the capacities. ^{7}Li NMR spectra of the Si–O–C composite materials had two resonances in the fully lithiated state, and one resonance could be attributed to less-ionic lithium species in the micropores. No voltage plateau was observed upon delithiation, and only a singular ^{7}Li NMR resonance was observed when the polysilanes alone were pyrolyzed. Although there was no decrease in the capacities, the voltage plateau disappeared with electrochemical cycling. Furthermore, different ^{7}Li NMR resonances from those observed in the first lithiation were clearly seen. These results indicate changes in the lithium environments in the Si–O–C composite materials.

1. Introduction

Rechargeable lithium-ion batteries have recently received considerable attention as very promising power sources with a high capacity and a high operating voltage, i.e., a high energy density [1]. Rechargeable lithium-ion batteries are essential for a number of portable applications such as cell phones and music players. For these batteries to be successfully used in a wider variety of applications, for example automotive applications, it is important to overcome some of the challenges related to their use. Much effort has thus been expended on enhancing aspects of battery performance such as energy density and cycle life. Anode materials have been a particular focus of attention because of the potential in this area for significantly improving the battery performance [2].

As previously reported [3–6], silicon oxycarbide (Si–O–C) glasses represent a new class of anode materials for rechargeable lithium-ion batteries. Many literature reports are available on methods of producing Si–O–C glasses (so-called black glasses) from sol/gels [7,8], silsesquioxanes [9], polysiloxanes [10], siloxane/silane aerosols [11], and silsesquioxane/siloxane copolymers [12]. Compared to SiO_2, one of the attributes of Si–O–C glasses is that divalent oxygen atoms are replaced by tetravalent carbon atoms. This makes these glasses more rigid and tough, offering improved physical and chemical properties. Si–O–C glasses usually contain free carbon as a second phase, which is responsible for their black appearance, along with a Si–O–C glass phase. The free carbon content is controlled using tailored prechar polymers with properties generally depending largely on the type of organic substituent [13,14]. It is believed that the Si–O–C glass phase is electrochemically active in lithium storage, thus delivering a higher capacity than that delivered by commercially successful graphite (theoretical capacity of 372 mA h g^{-1} as LiC_6). Although extensive research into carbon anode materials has been reported [15], no research has been reported clarifying the mechanism of electrochemical lithium storage in Si–O–C glasses.

We recently reported the first insights into the lithium storage mechanism in a Si–O–C composite material prepared by pyrolysis of a polymer blend of a phenyl-substituted branched polysilane, $(Ph_2Si)_{0.85}(PhSi)_{0.15}$ (Ph/Si ratio = 1.85), and polystyrene [16,17]. This composite material consists of graphene layers, Si–O–C glasses, and micropores, which enable both a capacity of more than 600 mA h g^{-1} and excellent cyclability to be achieved. The graphene layers act as major electrochemically active sites for lithium storage, and the Si–O–C glass phase and micropores are minor electrochemically active sites. The micropores in particular are expected to improve battery performance by acting as an electrochemical lithium storage site and alleviating volume changes on repeated lithium insertion and extraction. The architec-

* Corresponding author. Tel.: +81 42 677 2828; fax: +81 42 677 2828.
E-mail address: kanamura-kiyoshi@tmu.ac.jp (K. Kanamura).

0378-7753/$ – see front matter © 2010 Elsevier B.V. All rights reserved.
doi:10.1016/j.jpowsour.2010.06.077

Table 1
Nomenclature of char intermediates and pyrolysis products prepared in this study.

Prechar polymer	Char intermediate (600 °C)[a]	Pyrolysis product (1000 °C)[a]
1	CIP1	PP1
2	CIP2	PP2
3	CIP3	PP3
Polymer blend 1	CIB1	PB1
Polymer blend 2	CIB2	PB2
Polymer blend 3	CIB3	PB3

[a] The numbers correspond to those of the prechar polymers.

ture of the prechar polymers is important in controlling the final form of the pyrolysis products. Some structural changes, leading to micropore formation, occur in the course of polystyrene pyrolysis. Phenyl substituents also play important roles in this regard. Both polystyrene and phenyl substituents have so far been key to the incorporation of microporosity into a Si–O–C glass framework. However, there is a need for further understanding of micropore formation in glass frameworks from the viewpoint of materials design.

In this paper, our attention is focused on how polystyrene and different polysilane architectures influence micropore formation in the glass framework. Three methylphenyl-substituted branched polysilanes were studied: $(MePhSi)_{0.85}(MeSi)_{0.15}$ (**1**, Ph/Si ratio = 0.85); $(MePhSi)_{0.50}(Ph_2Si)_{0.30}(MeSi)_{0.20}$ (**2**, Ph/Si ratio = 1.1); $(MePhSi)_{0.70}(Ph_2Si)_{0.15}(MeSi)_{0.15}$ (**3**, Ph/Si ratio = 1.0). These polysilanes and their polystyrene polymer blends (1:1 by weight) were used as prechar polymers. Comparison of the pyrolysis behaviors enabled the aim of this study to be achieved. We also report the relationship between micropore formation and electrochemical lithium storage.

2. Experiments

2.1. Prechar polymers

The polystyrene (average degree of polymerization = 2000) used in this study was purchased from Wako Pure Chemical Industries. The polysilanes **1**–**3** used in this study were kindly supplied by the Dow Corning Corp. All the polysilanes were used as received. Neither product names nor product numbers were given to **1**–**3** because they were test samples. Typical polymer characteristics determined by gel permeation chromatography analysis (tetrahydrofuran, polystyrene standard) were as follows: $M_w = 2.16 \times 10^4$ for **1**, $M_w = 3.05 \times 10^3$ for **2**, and $M_w = 1.54 \times 10^4$ for **3**.

2.2. Preparation of the polymer blends

The detailed procedure has been described elsewhere [17]. The polymer blends were named polymer blend 1, 2, and 3, respectively. The numbers correspond to those of **1**–**3**, i.e., polymer blend 1 represents the prechar polymer prepared from a blend of **1** and polystyrene (1:1 by weight).

2.3. Pyrolysis of the polymer blends to 1000 °C

The pyrolysis procedure has been described in detail elsewhere [17]. In this study, we used char intermediates prepared at 600 °C under a nitrogen atmosphere. The char intermediates were milled and then sieved with a 300 mesh sieve; the nomenclature used for the intermediates is listed in Table 1. The char intermediates were pyrolyzed at 1000 °C under an argon atmosphere; the nomenclature used for the pyrolysis products is also listed in Table 1. In this study, CIP and CIB are the abbreviations for char intermediates made from the polymer and from the blend, respectively. PP and PB stand for pyrolysis products from the polymer and from the blend, respectively.

2.4. Materials analysis

Thermogravimetric analysis and differential thermal analysis (TGA/DTA) of the prechar polymers were carried out with a DTG-60 thermal analyzer (Shimadzu). The prechar polymers were heated to 900 °C at a rate of 2 °C min^{-1} under a nitrogen atmosphere. Analyses of the char intermediates and pyrolysis products were conducted using several techniques. X-ray diffraction (XRD) was performed using Cu Kα radiation (1.5418 Å) as the X-ray source (RINT 2200, Rigaku). Raman spectra were recorded on an NRS-1000 spectrometer (JASCO) with a 532-nm green laser source. Scanning transmission electron microscopy (STEM) images were captured with a JEM-3200FS (JEOL). Elemental analyses (CHN, O, and Si) of the pyrolysis products were performed by Sumika Chemical Analysis Service. Solid state ^{29}Si magic angle spinning nuclear magnetic resonance (MAS NMR) analyses were conducted at 59.6 MHz (AC300 spectrometer, Bruker). The detailed procedure has been explained elsewhere [17].

2.5. Electrochemical measurements

Electrochemical tests were performed using coin-type (either 2016 or 2032) cells. Prior to cell fabrication in an argon-filled glovebox, a working electrode (14-mm diameter) was prepared for each sample by mixing the active material, ketjen black, and poly(vinylidene fluoride) in a weight ratio of 85:5:10. The powdery mixture dispersed in *N*-methyl-2-pyrrolidinone (NMP, Wako Pure Chemical Industries) was coated on copper foil. After NMP removal, the working electrode was cut away from the copper foil. Lithium foil (15-mm diameter, Honjo Metal) was used as the counter electrode. The electrolyte was an ethylene carbonate/diethyl carbonate solution (1:1 by volume, Kishida Chemical) containing 1 mol dm^{-3} $LiPF_6$. A polypropylene sheet was sandwiched between the working electrode and the counter electrode as a separator. Galvanostatic lithiation/delithiation testing (37.2 mA g^{-1}) was conducted, using an HJ1010mSM8A (Hokuto Denko), at 30 °C. Lithiation/delithiation cycling was performed in the same manner. Lithiation/delithiation capacities were displayed with standard deviations.

2.6. ^{7}Li NMR analysis

Coin-type (2016) cells were fabricated in a way similar to that described above. The detailed procedures of sample preparation and ^{7}Li NMR analysis have been reported elsewhere [17]. The coin-type cells were dismantled in the glovebox after short-circuiting overnight, and then the working electrode for each sample was washed with dimethyl carbonate (DMC, Tomiyama Pure Chemical Industries). ^{7}Li NMR spectra were measured on a CMX-300 spectrometer (116.6 MHz, Chemagnetics) at room temperature. A 1 mol dm^{-3} aqueous LiCl solution was used as the external standard (0 ppm).

3. Results and discussion

3.1. Thermolysis

The similarity in the decomposition temperatures of **1**–**3** and polystyrene is expected to play a key role in micropore formation, as shown in Scheme 1. Pyrolysis to 1000 °C causes growth of both the free carbon and Si–O–C glass phases. TGA/DTA curves to 900 °C for **2** and polymer blend 2 are shown in Fig. 1. Both prechar polymers showed almost similar thermal decomposition behaviors, accompanied by a little weight loss, up to ca. 300 °C. However, significant

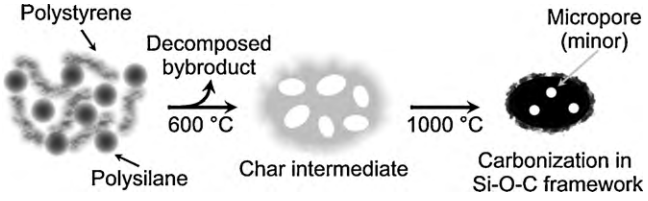

Scheme 1. Schematic model of micropore formation in Si–O–C glasses.

weight loss was observed at 300–450 °C, along with a characteristic endothermic peak, for polymer blend 2. This endothermic behavior pertains to the decomposition of polystyrene. Polysilane **2** and polystyrene therefore decompose in a similar temperature range. Above 600 °C, endothermic behaviors continued up to 900 °C in both prechar polymers. This is explained by growth of both the free carbon and Si–O–C glass phases. During thermal decomposition, emission of gaseous byproducts, such as benzene and silane compounds, is possible. A methylene insertion, resulting in Si–C–Si formation, may also occur in **1**–**3**, as observed for dimethylpolysilane [18].

According to our TGA/DTA results, most of the possible decomposed byproducts can be removed by thermolysis to 600 °C. We therefore first heat-treated a series of prechar polymers at 600 °C. Table 2 summarizes the thermolysis results for all the prechar polymers, along with the empirical formulae of the pyrolysis products. After heat treatment to 600 °C, the char yields were higher for **1**–**3** than for polymer blends 1–3 because of significant loss of polystyrene. Pyrolysis to 1000 °C led to little difference in char yields. Assuming that polystyrene is completely lost by thermal decomposition, the char yields in polymer blends 1–3 should be half those in **1**–**3**. However, polymer blends 1–3 obviously gave

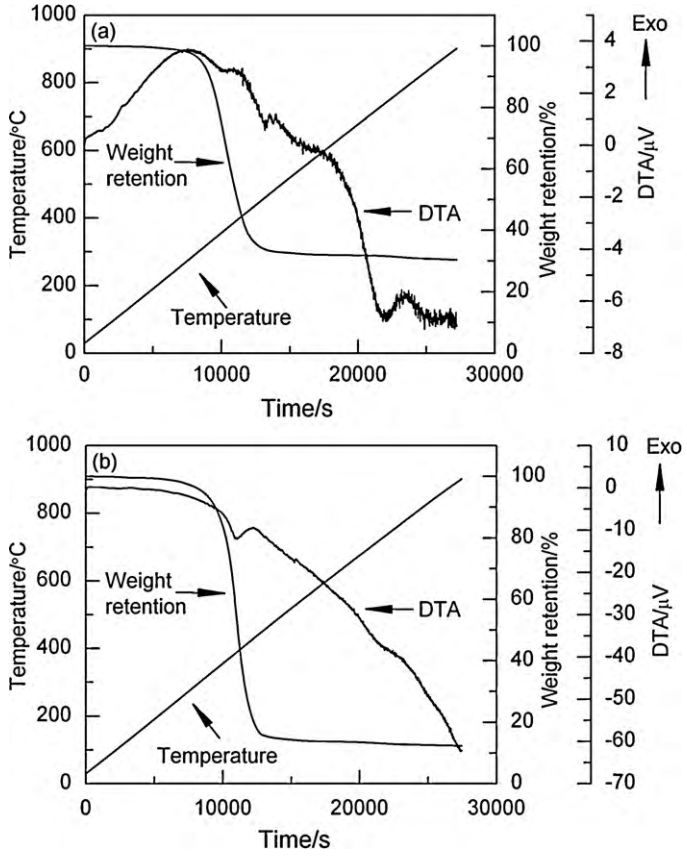

Fig. 1. TGA/DTA curves of (a) **2** and (b) polymer blend 2 to 900 °C.

Table 2
Summary of thermolysis of prechar polymers and empirical formulae of pyrolysis products.

Pyrolysis product	Char yield (%)		Empirical formula[b]
	600 °C	1000 °C[a]	
PP1	36	94	$SiO_{0.45}C_{2.93}$
PP2	38	96	$SiO_{0.32}C_{3.38}$
PP3	34	93	$SiO_{0.61}C_{2.74}$
PB1	22	95	$SiO_{0.35}C_{4.82}H_{0.15}$
PB2	23	95	$SiO_{0.40}C_{5.42}H_{0.22}$
PB3	22	95	$SiO_{0.29}C_{5.07}H_{0.21}$

[a] The char yields should be handled with caution because char intermediates may contain water adsorbed on the surfaces before pyrolysis.
[b] The nitrogen content was higher for PB1, PB2, and PB3 than for PP1, PP2, and PP3. We omit it from the empirical formulae because its maximum content was only 0.12%. The hydrogen content is ignored for PP1, PP2, and PP3 because of its very low content (0.01–0.09%)

higher than expected char yields. The empirical formulae confirm a higher carbon content in the PB series than in the PP series (Table 2), so polystyrene is likely to supply some of the free carbon. The hydrogen content also increased when polystyrene was blended. This may be associated with the presence of hydrogen on the edges of graphene layers of free carbon [19]. The results shown in Table 2 highlight the fact that oxygen is incorporated into the pyrolysis products, despite both prechar polymers being oxygen free. Because the inert gases used in this study were not absolutely pure, oxygen might have leaked into the furnaces during thermolysis.

Using the general formula $SiC_xO_{2(1-x)}$ [7], we can estimate the stoichiometric composition of Si–O–C glasses on the basis of the empirical formulae. In practice, however, Si–O–C glasses contain free carbon. Thus, yC (free carbon) should be added to the general formula. The stoichiometric Si–O–C glasses and the value of y in the pyrolysis products are shown in Table 3. The value of x varies in the range 0.70–0.86. Interestingly, the value of y in the PB series reached a value 2.3 times that in the PP series. This result also suggests that more free carbon can be delivered by decomposition of polystyrene.

3.2. Structural characterization

Regardless of polystyrene blending, no significant change in morphology was observed among the pyrolysis products. The particles were basically irregular in shape and broad in size. As shown in the STEM images of PP2 and PB2 (Fig. 2), there were also small flake-like particles.

Fig. 3 shows the Raman spectra of PB1 and PP1. In both cases, the pyrolysis products had two broad peaks assignable to G and D bands, the latter being the major band. It is therefore suggested that graphene layers with a high density of edges comprise the majority of the free carbon in both PB1 and PP1.

The XRD patterns of the char intermediates and the pyrolysis products are shown in Fig. 4a–c. Clear differences between the XRD

Table 3
Stoichiometric formulae of Si–O–C glasses and free carbon, $SiC_xO_{2(1-x)} + yC$, in pyrolysis products.

Pyrolysis product	Stoichiometric Si–O–C glasses[a]	y in free carbon[b]
PP1	$SiO_{0.45}C_{0.78}$	2.15
PP2	$SiO_{0.32}C_{0.84}$	2.54
PP3	$SiO_{0.61}C_{0.70}$	2.04
PB1	$SiO_{0.35}C_{0.83}$	3.99
PB2	$SiO_{0.40}C_{0.80}$	4.62
PB3	$SiO_{0.29}C_{0.86}$	4.21

[a] The stoichiometric Si–O–C glasses are estimated on the basis of the empirical formula and the general formula.
[b] y = the C/Si ratio in the empirical formula − x.

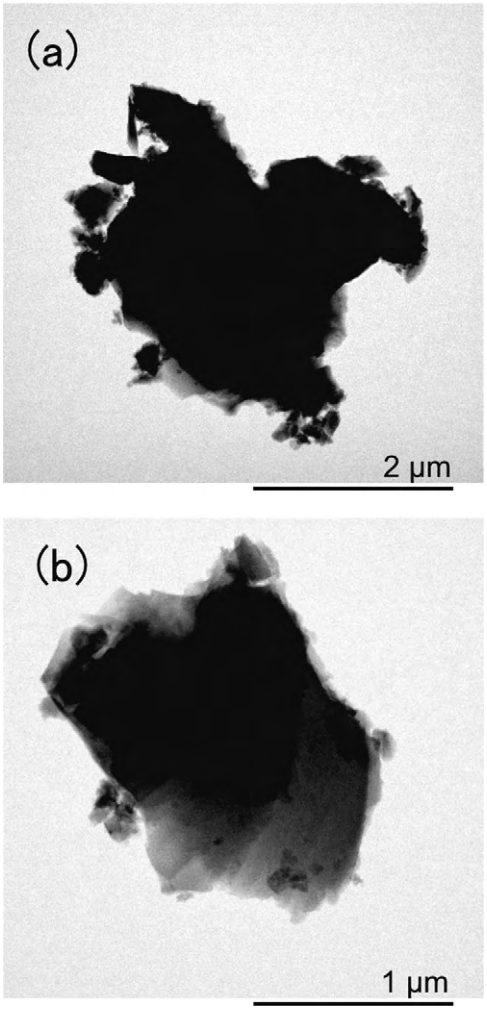

Fig. 2. STEM images of (a) PP2 and (b) PB2.

patterns of the CIP series and those of the CIB series were observed up to 2θ values of 30°. In particular, the intensity of the background was relatively high in the CIB series and fell steeply until $2\theta = 30°$. The high intensity of the background at lower 2θ regions is thought to be attributable to porosity in the CIB series. Hard carbon is known to present a similar XRD pattern because of its porous nature [20]. Pyrolysis to 1000 °C also led to different structural evolutions of the pyrolysis products. Given our pyrolysis conditions, it is reasonable to suppose that all the pyrolysis products would be amorphous. In

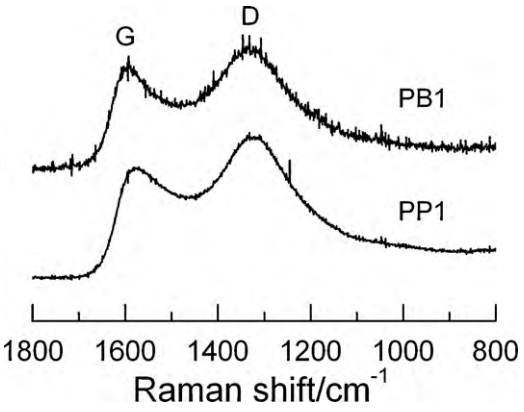

Fig. 3. Raman spectra of PP1 and PB1.

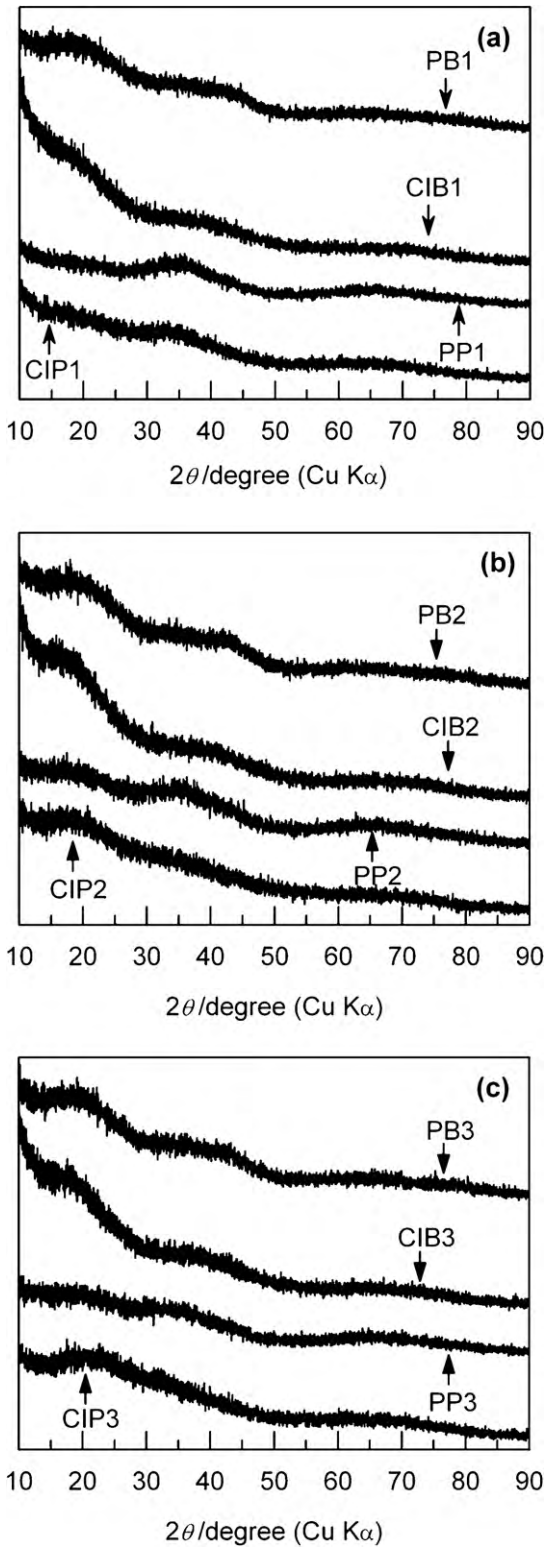

Fig. 4. XRD patterns of char intermediates and pyrolysis products: (a) CIP1, CIB1, PP1, and PB1; (b) CIP2, CIB2, PP2, and PB2; and (c) CIP3, CIB3, PP3, and PB3.

fact, no sharp diffraction peak was observed, but two broad peaks were visible in the XRD patterns. In the XRD patterns of PP1, PP2, and PP3, a broad peak at 2θ = ca. 36° was visible, which was ascribed to unorganized β-SiC. The presence of β-SiC was also suggested by the ^{29}Si MAS NMR spectrum of PP1 (Fig. 5), where broad resonances were identified mainly in four regions, indicating randomly distributed Si–O–C glass phases in short-range order. On the other

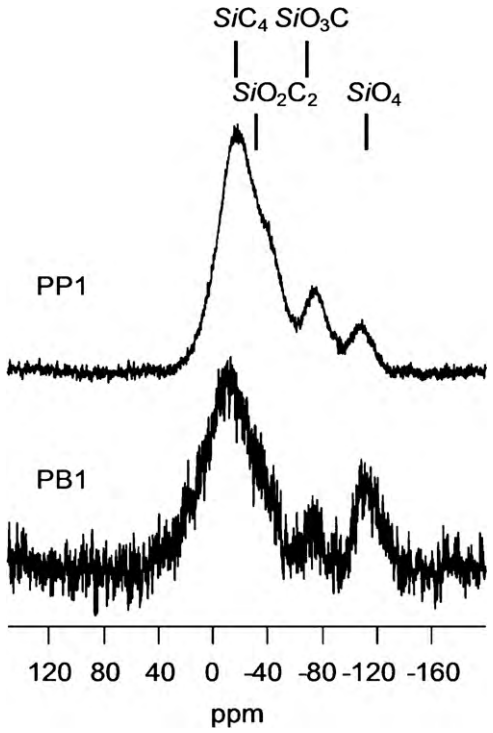

Fig. 5. ^{29}Si MAS NMR spectra of PP1 and PB1.

hand, two broad peaks at 2θ = ca. 21° and 43° were identified in the XRD patterns of PB1, PB2, and PB3. The peak at 2θ = ca. 21° is associated with amorphous SiO_2 [21] and the graphene layers with less stacking order. The ^{29}Si MAS NMR spectrum of PB1 also shows a resonance associated with a SiO_4 environment in the Si–O–C glass phase (Fig. 5). The other peak at 2θ = ca. 43° was assigned to the (10) diffraction of the graphene layers [22].

3.3. Electrochemical performance

Our analyses indicated several compositional and structural differences in the pyrolysis products. It would therefore be expected that the pyrolysis products would show different electrochemical behaviors in lithium storage. Our efforts were therefore devoted to highlighting the differences in electrochemical lithium storage of the pyrolysis products. Figs. 6 and 7 show the typical first and second lithiation/delithiation curves of the PP series and the PB series, respectively. In the first delithiation, PB1 and PB2 (546 ± 10 mA h g^{-1} and 565 ± 12 mA h g^{-1}) had higher capacities than those delivered by PP1 and PP2 (435 ± 5 mA h g^{-1} and 475 ± 10 mA h g^{-1}). Interestingly, however, PP3 and PB3 exhibited almost the same capacity in the first delithiation (523 ± 5 mA h g^{-1} and 520 ± 10 mA h g^{-1}). The first coulombic efficiencies of PP1, PP2, and PP3 were 63%, 63%, and 66%, respectively, and those of PB1, PB2, and PB3 were 71%, 73%, and 72%, respectively.

As shown in Figs. 6 and 7, some irreversible capacities corresponding to formation of a solid electrolyte interface (SEI) were observed at 0.7–1.0 V in the first lithiation of all the pyrolysis products. This SEI formation, mainly resulting from decomposition of the electrolyte, typically occurs in carbon materials such as graphite and disordered carbon [23]. One noteworthy feature that is clearly seen in the delithiation curves of PB1, PB2, and PB3, but not in those of PP1, PP2, and PP3, is a pseudo-voltage plateau at ca. 0.1 V. It is suggested that there are at least two different electrochemically active sites for lithium storage in PB1, PB2, and PB3. Furthermore, as seen in hard carbon, lithium species that are less ionic in nature can also be electrochemically inserted into micropores in PB1, PB2, and PB3.

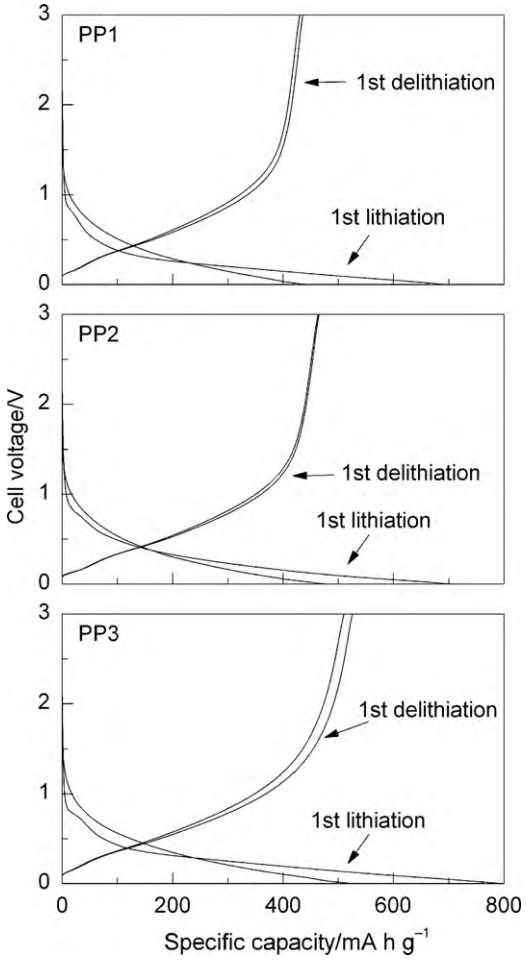

Fig. 6. The first and second lithiation/delithiation curves of PP1, PP2, and PP3.

It should be noted that the voltage plateau is short, indicating that the micropores are minor electrochemically active sites. This result emphasizes that the electrochemical lithium storage mechanism of the PP series and that of the PB series are very different. PP3 and PB3 had comparable capacities in the first delithiation up to 3 V, but the curve difference cannot be ignored. With regard to the first delithiation capacity up to 1 V, PB3 had a higher capacity than that delivered by PP3. This should favor PB3 as an anode material in view of the energy density of rechargeable lithium-ion batteries.

^{7}Li NMR analysis is a powerful technique in identifying the differences between electrochemically active sites for lithium storage in the pyrolysis products. Fig. 8 shows the ^{7}Li NMR spectra of PP1, PP2, and PP3 in the fully lithiated state. Because each electrode was washed with DMC before analysis, the ^{7}Li NMR resonance corresponding to $LiPF_6$ in the electrolyte was barely visible. The ^{7}Li NMR resonance associated with the SEI was also very small. There was a singular resonance centered at 12 ppm for PP1, 14 ppm for PP2, and 8 ppm for PP3 in the ^{7}Li NMR spectra. These ^{7}Li NMR resonances were all ascribed to lithium species of a more ionic nature than those of metallic lithium and LiC_6. Tatsumi et al. reported that mesocarbon microbeads (MCMBs) heat-treated at 700 °C and 1000 °C have a ^{7}Li NMR resonance centered at 7 ppm and 18 ppm, respectively, in the fully lithiated state [24]. Highly ordered graphitic structures cannot be formed in MCMBs at 700 °C and 1000 °C. Lithium cannot therefore be stored in the highly ordered graphitic structures but must be stored in disordered MCMB crystallites. It has also been reported that a ^{7}Li NMR resonance at ca. 7–13 ppm observed in hard carbon microbeads can be assigned to lithium stored in disordered carbon crystallites (interstitial spaces

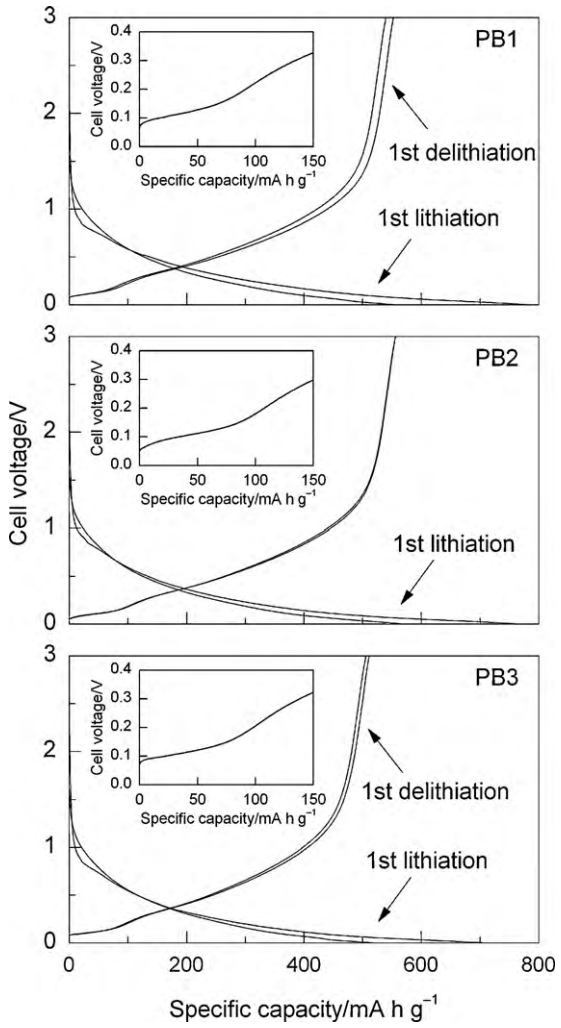

Fig. 7. The first and second lithiation/delithiation curves of PB1, PB2, and PB3. Insets are the magnified views of the first delithiation curves in the range 0–150 mA h g^{-1}. Note that the first delithiation curve almost overlaps the second delithiation curve in PB2.

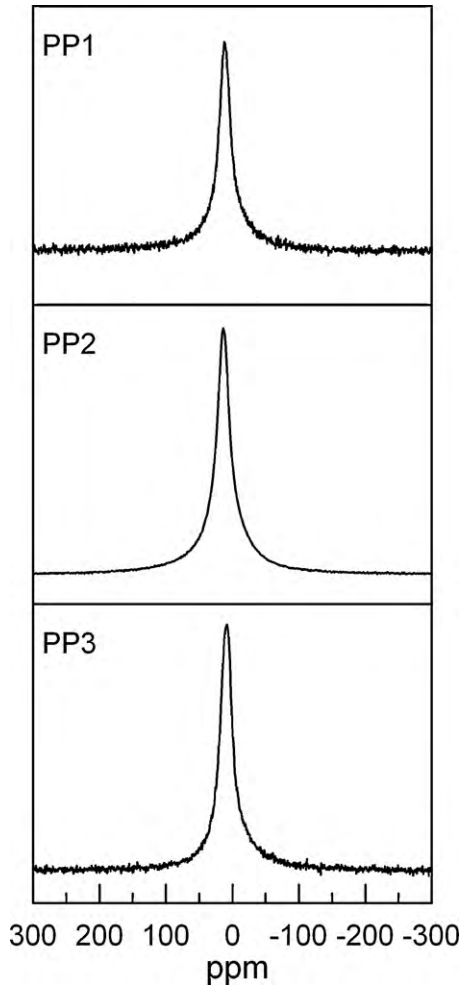

Fig. 8. ^{7}Li NMR spectra of PP1, PP2, and PP3 in the fully lithiated state.

and edges of the graphene layers) [25]. Given that PP1, PP2, and PP3 are amorphous, it is reasonable to suppose that lithium is stored in their disordered crystallites. If PP1, PP2, and PP3 have at least two electrochemically active sites, such as the Si–O–C glass phase and interstitial spaces or edges of the graphene layers, it is also possible that lithium is mobile between the two sites.

It is interesting that an unsymmetrical peak is clearly seen in the ^{7}Li NMR spectra of PB1, PB2, and PB3 in the fully lithiated state (Fig. 9). The broad peak was deconvoluted into two Lorentzian components. Fig. 9 also presents the deconvoluted spectra of the fully lithiated PB series. In the deconvoluted spectrum of fully lithiated PB1, two ^{7}Li NMR resonances are seen at 14 ppm (20%) and 28 ppm (80%), respectively. The broad peak in the ^{7}Li NMR spectrum of fully lithiated PB2 can be deconvoluted into two Lorentzian components at 13 ppm (21%) and 40 ppm (79%), respectively. In the deconvoluted spectrum of fully lithiated PB3, two ^{7}Li NMR resonances are also visible at 9 ppm (20%) and 45 ppm (80%), respectively. The ^{7}Li NMR resonances at the relatively high fields are close to the singular resonances observed in the fully lithiated PP series. Therefore, it is highly possible that these resonances contain a contribution from the same kind of lithium as that stored in the fully lithiated PP series. In the deconvoluted spectra of the fully lithiated PB series, the ^{7}Li NMR resonances at the relatively low fields make a major contribution, and their full width at half maximum is more than three times that of the resonances at the relatively high fields. The relatively low-field resonances are seen exclusively in the fully lithiated PB series, and thus our ^{7}Li NMR analysis establishes the emergence of different electrochemically active sites for lithium storage.

In the fully lithiated state, MCMBs heat-treated above 2000 °C showed two ^{7}Li NMR resonances at ca. 27 ppm and 45 ppm; these were assigned to lithium in the turbostratic structure and the LiC_6 phase of graphitic structures, respectively [24]. In particular, the turbostratic structure, estimated to be $Li_{0.2}C_6$, had low electrochemical lithium storage capability [24]. In this study, the PB series was prepared at quite a low temperature of 1000 °C, so even the turbostratic structure would not be realistic. This idea therefore apparently makes it difficult to apply the lithium storage mechanism of the MCMBs to the PB series. According to a previous study [25], hard carbon microbeads produced a similar broad resonance, which was assigned to lithium species with less-ionic natures, at 36 ppm. In addition, exchange of lithium nuclei was observed between micropores and other active sites in the fully lithiated Si–O–C composite material on the NMR timescale [17]. On the basis of our structural analysis results, the microstructure of the PB series is thought to be similar to that of hard carbon rather than that of soft carbon such as MCMBs. The relatively low-field resonances therefore indicated the presence of lithium species which were rapidly exchanging, on the NMR timescale, between the micropores and other active sites. According to our electrochemical testing and ^{7}Li NMR analysis, structural differences can be produced by polystyrene blending: (1) the content of phenyl substituents in **1**–**3**,

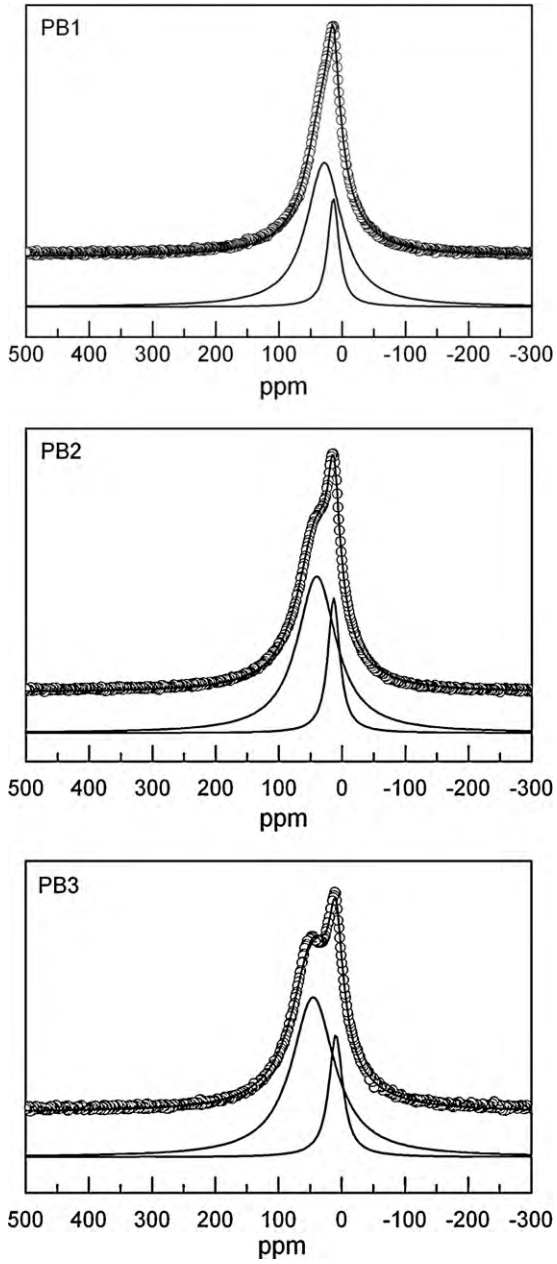

Fig. 9. ^{7}Li NMR spectra of PB1, PB2, and PB3 in the fully lithiated state. Top: (○) experimental, (–) simulated; bottom: deconvoluted.

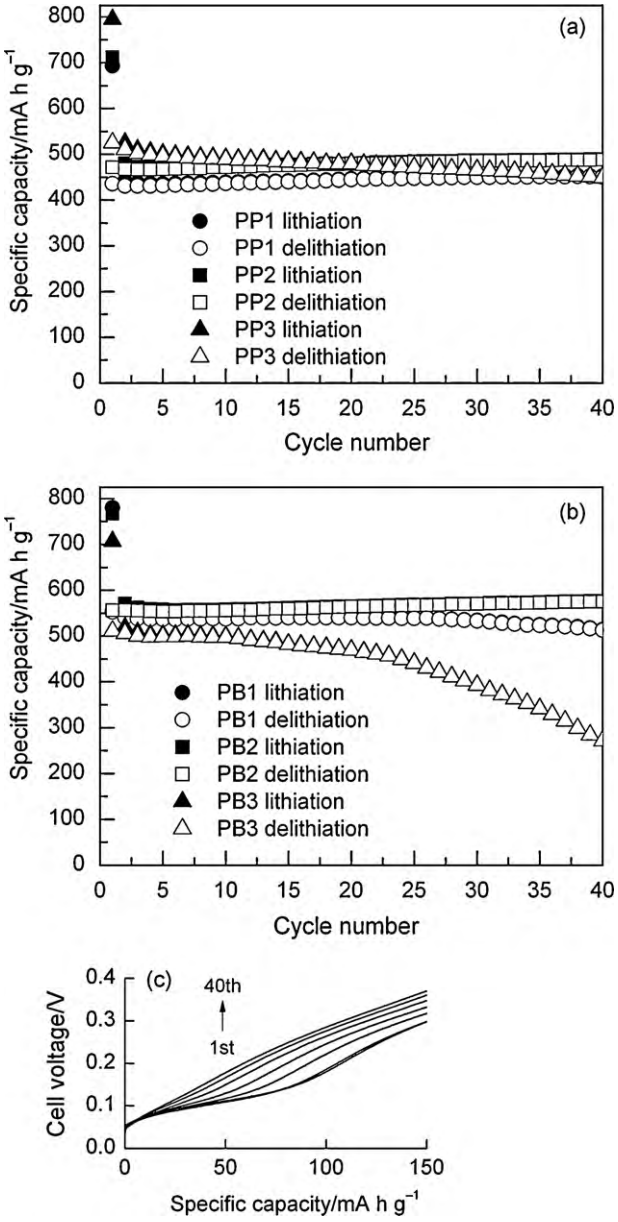

Fig. 10. (a) Cycling performance of PP1, PP2, and PP3; (b) cycling performance of PB1, PB2, and PB3; and (c) enlarged view of delithiation curves (the 1st, 2nd, 5th, 10th, 20th, 30th, and 40th) of PB2 in the range 0–150 mA h g^{-1}.

with Ph/Si ratios = 0.85–1.1, is not enough to form micropores; (2) polystyrene plays a key role in micropore formation.

We believe that micropores also enhance cyclability. Fig. 10a and b depicts the cycling performance of the PP series and the PB series, respectively. While PP1 and PP2 ensured good cyclability, the capacity of PP3 gradually decreased from that in the early cycles. Interestingly, PB1 and PB2 had good cyclability, but PB3 showed a very short cycle life. The poor cycling performance of PB3 is of great interest. Because both PP3 and PB3 differed from the other pyrolysis products in terms of electrochemical performance, as mentioned above, the exclusive poor cyclability of PB3 may be associated with minor structural differences that have not as yet been understood. On the basis of these results, it appears that micropores do not necessarily improve the cyclability of the pyrolysis products. Our lithiation/delithiation cycling test, however, demonstrated that PB1 and PB2 can give high lithium storage capacity and good cyclability.

On repeated lithiation and delithiation, the distinctive voltage plateau completely disappeared in the delithiation curves of PB1, PB2, and PB3. Although no decrease in the capacity of PB2 was observed upon delithiation, the voltage plateau almost disappeared after 30 cycles (Fig. 10c). Interestingly, this phenomenon was accompanied by a gentle increase in the delithiation voltage. If the voltage plateau arises from extraction of less-ionic lithium species stored in micropores of PB1, PB2, and PB3, the disappearance of the plateau means that some structural changes occur in PB1, PB2, and PB3; the micropores lose electrochemical activity on repeated lithium insertion and extraction. Some new electrochemically active sites for lithium storage must offset the loss of the micropores to generate almost equivalent capacities. To obtain more information on the disappearance of the voltage plateau on repeated lithiation and delithiation, a ^{7}Li NMR spectrum was recorded for PB2 in the fully lithiated state after 18 cycles (Fig. 11a). Fully lithiated PB2 has ^{7}Li NMR resonances quite different from those shown in Fig. 9. The ^{7}Li NMR resonances simulated in the

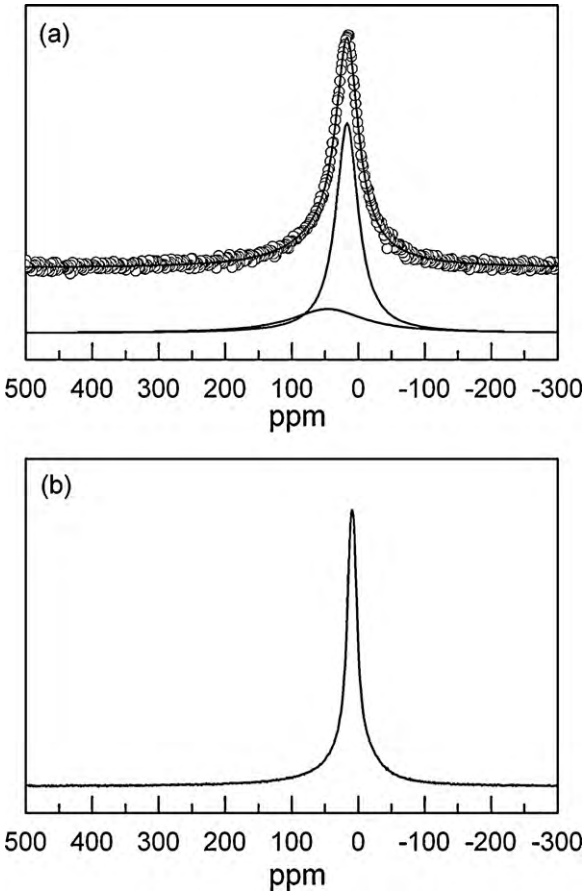

Fig. 11. ^{7}Li NMR spectra of (a) PB2 in the fully lithiated state after 18 cycles and (b) PP3 in the fully lithiated state after 20 cycles. Top in (a): (○) experimental, (–) simulated; bottom in (a): deconvoluted.

spectrum are 17 ppm (73%) and 46 ppm (27%), respectively. It is evident that the dominant shoulder peak (40 ppm in Fig. 9) becomes minor at the lower field. This spectral change strongly supports the idea that PB2 no longer possesses exactly the same electrochemically active sites for lithium storage as those observed in the first lithiation. This agrees well with the disappearance of the voltage plateau upon delithiation. On the other hand, fully lithiated PP3 shows little spectral change (9 ppm) in the ^{7}Li NMR analysis (Fig. 11b). The electrochemically active sites in PP3 are unlikely to be changed by repeated lithiation and delithiation.

4. Conclusions

We examined the influence of polystyrene and the phenyl substituents in $(MePhSi)_{0.85}(MeSi)_{0.15}$ (**1**), $(MePhSi)_{0.50}(Ph_2Si)_{0.30}(MeSi)_{0.20}$ (**2**), and $(MePhSi)_{0.70}(Ph_2Si)_{0.15}(MeSi)_{0.15}$ (**3**) on the formation of micropores in Si–O–C glasses. Thermal analyses showed that polystyrene and **1**–**3** mainly decomposed at almost the same temperature. This behavior should affect the high-temperature chemistry of the prechar polymers. Electrochemical measurements were also carried out to evaluate the pyrolysis products as potential anode materials for rechargeable lithium-ion batteries. The pyrolysis products were grouped into two types: (1) a PB series prepared from the polymer blends; (2) a PP series prepared from **1** to **3** alone. The PB series had higher capacities than those delivered by the PP series, highlighting the benefits of polystyrene-driven micropore formation; a distinctive pseudo-voltage plateau at ca. 0.1 V upon delithiation was observed only with the PB series. The voltage plateau was short, but indicated the presence of micropores as minor electrochemically active sites for lithium storage. ^{7}Li NMR spectra also showed that the PB series and the PP series had quite different electrochemical lithium storage mechanisms. The fully lithiated PP series exhibited a singular ^{7}Li NMR resonance similar to that observed in fully lithiated soft carbon. Two ^{7}Li NMR resonances, on the other hand, can be simulated in the ^{7}Li NMR spectra of the fully lithiated PB series; one is close to the singular resonance seen in the fully lithiated PP series, and the other could contain a contribution from less-ionic lithium species stored in the micropores. The structural and electrochemical results supported the idea that pyrolysis of **1**–**3** with Ph/Si ratios = 0.85–1.1 did not lead to micropore formation, but the polymer blends successfully incorporated microporosity into the Si–O–C host frameworks. Interestingly, after several tens of lithiation/delithiation cycles, the voltage plateau could no longer be seen in some of the PB series materials, despite their stable capacities. ^{7}Li NMR analysis suggested that changes occurred in the lithium local environments.

Acknowledgements

The authors thank Dr. K. Tatsumi, M. Nakajima, and Dr. H. Sakaebe for helpful discussions and assistance with ^{7}Li NMR analysis. We are also grateful to K. Eguchi for ^{29}Si MAS NMR analysis and Y. Misaki for STEM measurements.

References

[1] M. Armand, J.-M. Tarascon, Nature 451 (2008) 652.
[2] M. Winter, J.O. Besenhard, Electrochim. Acta 45 (1999) 31.
[3] W. Xing, A.M. Wilson, G. Zank, J.R. Dahn, Solid State Ionics 93 (1997) 239.
[4] W. Xing, A.M. Wilson, K. Eguchi, G. Zank, J.R. Dahn, J. Electrochem. Soc. 144 (1997) 2410.
[5] H. Tamai, H. Sugahara, H. Yasuda, J. Mater. Sci. Lett. 19 (2000) 53.
[6] H. Konno, T. Morishita, S. Sato, H. Habazaki, M. Inagaki, Carbon 43 (2005) 1111.
[7] G.D. Sorarù, G. D'Andrea, R. Campostrini, F. Babonneau, G. Mariotto, J. Am. Ceram. Soc. 78 (1995) 379.
[8] Q. Liu, W. Shi, F. Babonneau, L.V. Interrante, Chem. Mater. 9 (1997) 2434.
[9] F.I. Hurwitz, P. Heimann, S.C. Farmer, D.M. Hembree Jr., J. Mater. Sci. 28 (1993) 6622.
[10] R.J.P. Corriu, D. Leclercq, P.H. Mutin, A. Vioux, J. Mater. Sci. 30 (1995) 2313.
[11] Y. El Kortobi, J.-B. d'Espinose de la Caillerie, A.-P. Legrand, X. Armand, N. Herlin, M. Cauchetier, Chem. Mater. 9 (1997) 632.
[12] R.A. Mantz, P.F. Jones, K.P. Chaffee, J.D. Lichtenhan, J.W. Gilman, I.M.K. Ismail, M.J. Burmeister, Chem. Mater. 8 (1996) 1250.
[13] D.A. White, S.M. Oleff, R.D. Boyer, P.A. Budinger, J.R. Fox, Adv. Ceram. Mater. 2 (1987) 45.
[14] G.T. Burns, R.B. Taylor, Y. Xu, A. Zangvil, G.A. Zank, Chem. Mater. 4 (1992) 1313.
[15] J.R. Dahn, T. Zheng, Y. Liu, J.S. Xue, Science 270 (1995) 590.
[16] H. Fukui, H. Ohsuka, T. Hino, K. Kanamura, Chem. Lett. (2009) 86.
[17] H. Fukui, H. Ohsuka, T. Hino, K. Kanamura, ACS Appl. Mater. Interfaces 2 (2010) 998.
[18] S. Yajima, J. Hayashi, M. Omori, K. Okamura, Nature 261 (1976) 683.
[19] T. Zheng, Y. Liu, E.W. Fuller, S. Tseng, U. von Sacken, J.R. Dahn, J. Electrochem. Soc. 142 (1995) 2581.
[20] Y. Liu, J.S. Xue, T. Zheng, J.R. Dahn, Carbon 34 (1996) 193.
[21] L. Wang, A. Lu, C. Wang, X. Zheng, D. Zhao, R. Liu, J. Colloid Interface Sci. 295 (2006) 436.
[22] C.L. Burket, R. Rajagopalan, H.C. Foley, Carbon 46 (2008) 501.
[23] K. Kanamura, S. Shiraishi, H. Takezawa, Z. Takehara, Chem. Mater. 9 (1997) 1797.
[24] K. Tatsumi, T. Akai, T. Imamura, K. Zaghib, N. Iwashita, S. Higuchi, Y. Sawada, J. Electrochem. Soc. 143 (1996) 1923.
[25] R. Alcántara, G.F. Oritz, P. Lavela, J.L. Tirado, R. Stoyanova, E. Zhecheva, Chem. Mater. 18 (2006) 2293.